

Turbulent Dissipation Challenge

Problem Description

Tulasi N Parashar¹, Chadi Salem², Robert Wicks³, Homa Karimabadi⁴, S Peter Gary⁵
Benjamin Chandran⁶, William H Matthaeus⁷

The Goal

The goal of this document is to present a detailed description of the goals, simulation setup and diagnostics for the "Turbulent Dissipation Challenge" (<http://arxiv.org/abs/1303.0204>) as discussed in the Solar Heliospheric & INterplanetary Environment (SHINE) 2013 workshop, American Geophysical Union's Fall Meeting 2013 and the accompanying antenna meeting in Berkeley.

Contents

1	Motivation	1
2	Definition of Goals	2
3	Problem Description	3
3.1	Intermittent Structures	3
3.2	Wave Physics	4
4	Common Diagnostics	6
4.1	Intermittent Structures	7
4.1.1	PDFs of Increments	7
4.1.2	Scale Dependent Kurtosis	8
4.1.3	Structure Functions and their scaling exponents	8
4.2	Wave Physics	8
4.2.1	Dispersion Analysis	9
4.2.2	Damping Rate	9
4.2.3	Compressibility	10
4.2.4	The Electric to Magnetic Field Ratio	10
4.3	Comparison to Observations	11
5	Conclusion	11
A	Wave vectors for the KAW runs	11

¹CalTech NASA Jet Propulsion Laboratory, Pasadena, Currently at University of Delaware, Newark, DE

²Space Science Laboratory, University of California, Berkeley

³NASA Goddard Space Flight Center, Greenbelt, MD

⁴Department of Electrical and Computer Engineering, University of California, San Diego

⁵Space Science Institute, Boulder

⁶University of New Hampshire, Durham, NH

⁷University of Delaware, Newark, DE

1 Motivation

The near Earth space is a dynamic system where plasma coming from the Sun, aka solar wind, and Earth's plasma sphere, aka magnetosphere, interact. The dynamics of this system affects not only our spacecraft and astronauts but also wireless communications and in some extreme cases, the electrical grids on Earth. It is very important to have good predictive capabilities for this system. An integral part of the system is the medium that connects Sun and Earth: the solar wind.

The solar wind is observed to be turbulent. By this we mean that the energy at the largest scales is "cascaded" to smaller scales via nonlinear interactions creating a broad-band spectrum of incoherent fluctuations in fields and flows. The distribution of energy at various scales usually follows a power law (e.g. Kolmogorov (1941)). The solar wind magnetic energy spectrum obeys the Kolmogorov power law in the "inertial range" (e.g. Coleman (1968); Matthaeus and Goldstein (1982); Goldstein et al. (1995)), which covers scales larger than the proton inertial length $d_i = c/\omega_{pi}$ ($\sim \rho_i$) where c is the speed of light and ω_{pi} is the proton plasma frequency. At scales close to d_i a break in the spectrum occurs and it becomes steeper (e.g. Sahrhoui et al. (2009); Alexandrova et al. (2012)), indicating a loss of energy at the proton scales. This is consistent with the observations of proton temperature being larger than that expected from a purely adiabatic expansion (e.g. Wang and Richardson (2001)).

Exactly how the energy in flow and electromagnetic fluctuations is converted to the thermal degrees of freedom of the protons is still debated. The mechanism has to be largely collisionless and has to explain features observed in the solar wind, e.g. anisotropic heating of the protons (e.g. Marsch (2006) and references therein). We outlined the proposed mechanisms and the related debate in our earlier white paper and will only summarize them here for the sake of brevity. For a detailed discussion please refer to Parashar and Salem (2013).

The important processes proposed for explaining the anisotropic heating of protons can be broadly divided into two categories, wave damping mechanisms and non-wave mechanisms.

Wave damping mechanisms include cyclotron damping (e.g. Hollweg and Isenberg (2002) and references therein), Landau damping (e.g. Schekochihin et al. (2009) and references therein). The non-wave mechanisms involve either low frequency intermittent structures like current sheets and reconnection sites (e.g. Sundkvist et al. (2007); Parashar et al. (2009, 2011); Osman et al. (2011); Wan et al. (2012); Karimabadi et al. (2013)) or ideas like stochastic heating (e.g. Chandran et al. (2010); Xia et al. (2013); Bourouaine and Chandran (2013)). There are problems associated with these mechanisms that make it difficult to propose one of the mechanisms as the dominant mechanism for heating solar wind protons. Cyclotron heating requires sufficient energy at high k_{\parallel} but plasma turbulence with a mean magnetic field (like the solar wind) becomes highly anisotropic with most of the energy residing in high k_{\perp} . There is still no consensus on how to provide energy to high enough k_{\parallel} for this mechanism to be valid. Landau damping inherently produces high T_{\parallel} and hence would provide parallel proton heating instead of perpendicular heating. Intermittent structures have been shown to have a strong correlation with highly anisotropic heating but the cause-effect relation is not completely understood and the

exact details of how the heating takes place are debated.

We anticipate that most of these processes should be active in solar wind at any given moment. The fundamental problem of interest is to quantify the contributions of various processes under given solar wind conditions. The purpose of “Turbulent Dissipation Challenge” is to bring the community together and take a decisive step in this direction. This is a particularly hard problem and there are many caveats that need to be considered before making a full attempt at addressing this issue.

2 Definition of Goals

The underlying issue that has hindered a constructive progress in answering the question of dissipation in solar wind is a lack of cross comparison between results from various studies.

- Most of the numerical studies are done using models that are vastly different in their underlying assumptions and numerical schemes. E.g. electron magnetohydrodynamics (EMHD) is the fluid description of the electron dynamics considering protons to be an immobile neutralizing background, hybrid particle in cell (hybrid-PIC) treats protons as particles and electrons as a neutralizing fluid (usually massless and isothermal) whereas gyrokinetics is a Vlasov Maxwell system in which the gyro motion of the particles has been averaged out from the system. These are just three examples from many possible models e.g. MHD, Hall MHD, Hall-FLR MHD, EMHD, RMHD, ERMHD, Landau Fluid, Hybrid PIC, Hybrid Eulerian Vlasov, Full PIC, Full Eulerian Vlasov, Gyrokinetics.

Most of the times, the studies performed using these different models do not have the same initial conditions or even same parameters. Hence it is not possible to cross compare the findings of these studies.

- Similar problems are present with spacecraft data analysis. The data can be chosen from many spacecraft, e.g. WIND, CLUSTER, ACE, Helios, Ulysses, Voyager to name a few. Even if the data is from the same spacecraft, the intervals chosen could be vastly different ranging from fast wind to slow wind to all inclusive.

Also, the analysis techniques have not been methodically benchmarked against other analysis techniques and simulations

The above mentioned problems call for a systematic cross comparison study where different simulation models are used to study the exact same initial conditions under as close physical and numerical parameter regimes as possible. Artificial spacecraft data from these simulations can then be used to benchmark different spacecraft data analysis techniques with simulations as well as with each other.

The first step of the endeavor is to understand how well different codes capture the essential underlying physics. As discussed above, the essential ingredients of plasma turbulence that are expected to play a significant role are intermittent structures and wave damping. Hence we define the first step of this endeavor to be the following:

With given initial conditions and physical parameters, how do different simulation models cross compare in capturing the physics of: i) intermittent structures and ii) wave damping?

To do so, multiple simulation codes will perform two problems with the exact same physical parameters and as close numerical parameters as possible. The two problems will be:

- First problem will be designed to generate strong turbulence with intermittent structures.
- Second problem will be designed to have a spectrum of waves with a given damping rate.

By performing these simulations using different simulation models and performing the same set of diagnostics, we will be able to quantitatively cross compare the results from different models. This will help us better understand how well different codes capture the physics of interest. Artificial spacecraft data will be provided to observers in order to establish a system that will be used to address physics questions at a later stage in the challenge.

We now go on to describe the problem parameters and initial conditions in detail.

3 Problem Description

The conditions for the first simulations will be chosen to represent solar wind at 1 AU. Hence a plasma $\beta \sim 0.6$ will be used along with $T_e = T_i$, $m_e/m_i = 0.01$, $dt = 10^{-3}\omega_{ci}^{-1}$. To keep the computational costs down, the simulations will be performed in 2.5D, i.e. the simulation dynamics will be in a plane but with 3D components for all the vectors.

We understand that full 3D simulations with out of plane couplings are required for a complete description of the dynamics, but given the computational enormity of these models, large 3D kinetic simulations will not be possible. A compromise between inclusion of out of plane couplings and Reynolds number of the system (proportional to the system size) has to be made.

Observations show that the anisotropy and intermittency grow with the width of the inertial range e.g. Wicks et al. (2010, 2012); Greco et al. (2008); Wu et al. (2013). Hence, we choose to work with systems with a reasonable Reynolds number to compare the codes. After the code comparison, the critical simulations can be better designed in 3D.

3.1 Intermittent Structures

These simulations will study the intermittent structures that emerge from the nonlinear development of a Kelvin-Helmholtz instability (e.g. Chandrasekhar (1961); Miura and Pritchett (1982); Karimabadi et al. (2013)). The Kelvin Helmholtz instability gives rise to large scale vortices and current sheets. As the vortices roll up, the current sheets get thinner and give rise to secondary tearing instabilities. This generates a turbulent "soup" of current sheets ranging in scales from proton to electron scales. The ease of setting

up KH and the broad range of turbulent current layers generated by it make it an ideal candidate for studying how well different codes capture intermittent physics.

We will follow the setup used in Karimabadi et al. (2013) with a slight modification for this test. The initial density n_0 and magnetic field \mathbf{B}_0 will be uniform. \mathbf{B}_0 will be inclined w.r.t. the plane of simulation such that $\mathbf{B} = B_0[\mathbf{e}_y \sin \theta + \mathbf{e}_z \cos(\theta)]$ with $\theta = 2.86^\circ$. To allow for use of periodic boundary conditions, we will use a double shear layer of flow. The shears will be present at $y = 0.25L_y, 0.75L_y$ with the shear layer flow defined as $\mathbf{U} = U_0 \tanh(2\pi(y - 0.25)/2L_V) \mathbf{e}_y$ for the layer at $y = 0.25L_y$ and $\mathbf{U} = -U_0 \tanh(2\pi(y - 0.75)/2L_V) \mathbf{e}_y$ for the layer at $y = 0.75L_y$ where $U_0 = 10V_A^*$, $V_A^* = B_0 \sin(\theta) / \sqrt{4\pi n_0}$ and $L_V = 4d_i$, $\beta = 0.6$, $\omega_{pe}/\omega_{ce} = 1.5$. The system size will be $L_x = 125.d_i$, $L_y = 125.d_i$, $N_x = 2048$, $N_y = 2048$. Also a perturbation of the form $\delta\mathbf{U} = \delta U_0 \sin(0.5y/L_V) \exp(-x^2/L_V^2)$, where $\delta U_0 = 0.15U_0$, will be added in the shear layer to expedite the growth of the instability.

For PIC codes, excess particles will be loaded into the transition layer to balance the electric field because of the cross field flow $\mathbf{E} = (B_0 U_0 / c) \tanh(x/L_V) \mathbf{e}_x$.

3.2 Wave Physics

If linear Vlasov theory can provide a guidance to the nature of fluctuations at kinetic scales, we can have two main possibilities: the fluctuations could behave predominantly like Kinetic Alfvén Waves or like whistler waves. It is generally agreed upon that the fluctuations close to proton inertial scales behave like KAWs e.g. Leamon et al. (1999); Bale et al. (2005); Sahraoui et al. (2010); He et al. (2012); Salem et al. (2012); TenBarge et al. (2012). However whether KAWs dominate down to electron scales or not is debated e.g. Howes et al. (2008); Sahraoui et al. (2009); Podesta et al. (2010); Gary et al. (2008); Shaikh and Zank (2009).

The Turbulent Dissipation Challenge addresses the dissipative processes at the proton scales. Also, at the first step, the emphasis is on comparing the capability of different simulation codes to capture wave physics. Hence, for comparing wave physics, the initial condition will be a spectrum of Kinetic Alfvén Waves (KAWs). The idea is to study how well do different codes capture wave dynamics. The critical simulations to be done at later stages will have more realistic composition of fluctuations.

For the first step, we propose following constraints/ requirements on the problem:

- As the challenge is focussed on the proton inertial scales, the initial condition should be a spectrum of KAWs around $kd_i \sim 1$.
- The box should have at least a decade in the inertial range above proton scales and should also resolve at least a decade below the proton inertial length.
- The problem should be doable in reasonable time on modern computing clusters.

Given the above constraints, $L_x = L_y = 125.c/\omega_{pi}$, $N_x = N_y = 2048$, will give us $\Delta x = 0.061$ corresponding to about 16 grid points across d_i and 3 grid points across $2d_e$. This will also correspond to the spectral range of $k_{min} = 0.05$ and $k_{max} = 102.94$. To decide on the values of $|k|$ to be used in the initial spectrum, we look at the dispersion curves for

KAWs, calculated using linear vlasov theory (e.g. Gary (1986, 2005)), with the parameters: $\beta = 0.6$, $V_A/c = 1/15.$, $m_e/m_i = 0.01$, for a few different angles of propagation.

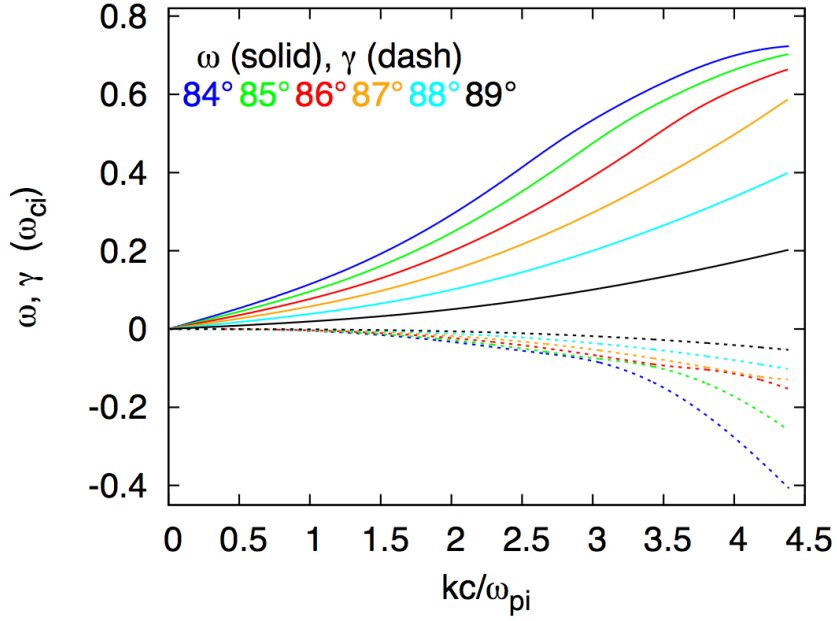


Figure 1: Dispersion curves for KAWs propagating at various angles in a proton electron Maxwellian plasma with $\beta = 0.6$, $T_e = T_i$, $m_e/m_i = 0.01$, $V_A/c = 1/15.$. Solid lines represent real frequency and dashed lines represent the damping.

Figure 1 shows the dispersion curves for various angles of propagation of KAWs in a Maxwellian proton-electron plasma with $\beta = 0.6$, $T_e = T_i$, $m_e/m_i = 0.01$, $V_A/c = 1/15.$ Almost all of these curves are dispersive at $kc/\omega_{pi} \sim 1.$ and have very low and comparable damping rates. We choose the window $0.5 \leq k \leq 1.5$ which will give us not only dispersive waves, similar damping rates but also ~ 66 grid points across the smallest wavelength in the initial spectrum. This means that the shorter wavelengths generated by the cascade will have sufficient resolution across them.

The next constraint on the choice of $|k|$ values is that the k_{\parallel} and k_{\perp} should be excitable on discrete grid points for periodicity. With this in mind, we choose the following 8 numbers for $k_x \equiv k_{\parallel}$, $k_y \equiv k_{\perp}$. The table shows values in units of kd_i as well as number of wavelengths in the box in parenthesis.

$k_x d_i$	$k_y d_i$	$ k $	θ_{kB}
0.05 (1)	0.50 (10)	0.0502	84.8294
0.05 (1)	0.65 (13)	0.6519	85.6013
0.05 (1)	0.80 (16)	0.8016	86.4237
0.05 (1)	0.95 (19)	0.9513	86.9872
0.05 (1)	1.10 (22)	1.1011	87.3974
0.05 (1)	1.25 (25)	1.2510	87.7094
0.05 (1)	1.40 (28)	1.4009	87.9546
0.05 (1)	1.55 (31)	1.5508	88.1524

The parallel (k_x) and perp (k_y) wavenumbers in units of kd_i as well as the number of wavelengths in the box (in parenthesis). Corresponding $|k|$ and θ_{kB} are also shown.

The initial condition will be a spectrum of KAWs with above mentioned $|k|$ and θ_{kB} created using the prescription in section 3 of Gary and Nishimura (2004). The initial field fluctuations are written as:

$$\delta\mathbf{B}(x, t = 0) = \sum_{\alpha=x,y,z} \hat{\mathbf{e}}_{\alpha}(\delta B_{\alpha})_0 \sin(k_x x + k_y y + \phi_{B\alpha}) \quad (1)$$

$$\delta\mathbf{E}(x, t = 0) = \sum_{\alpha=x,y,z} \hat{\mathbf{e}}_{\alpha}(\delta E_{\alpha})_0 \sin(k_x x + k_y y + \phi_{E\alpha}) \quad (2)$$

$$\delta\mathbf{v}_j(x, t = 0) = \sum_{\alpha=x,y,z} \hat{\mathbf{e}}_{\alpha}(\delta v_{j\alpha})_0 \sin(k_x x + k_y y + \phi_{vj\alpha}) \quad (3)$$

where the individual components are provided by the linear Vlasov code (Gary (1986)). The phases are chosen randomly. We expect the kinetic codes to quickly adjust the phases to the real phases of the fluctuations. The total amplitude of the fluctuations will be such that $|\delta B|^2/B_0^2 \sim 0.1$. The wave vectors output from the linear Vlasov code (Gary (1986)) for the given parameters are listed in the appendix.

4 Common Diagnostics

To facilitate a quantitative comparison between different models, a common set of diagnostics will be performed on the simulations. Below we outline the potential diagnostics that are reasonably straightforward to implement. A few diagnostics common to all the simulations would be:

- All kinetic simulations will plot change in thermal energy of protons as a fraction of free energy available at the beginning of the simulation. Where possible, anisotropy as defined by T_{\perp}/T_{\parallel} , with \perp and \parallel defined w.r.t. mean field, should also be plotted. As an example, figure 2 shows the change in thermal energy as well as the anisotropy for three hybrid simulations of Orszag-Tang vortex (OTV) with different equation of state for electrons (for details see Parashar et al. (2014)).

This way of plotting makes the results independent of the units used in the simulation code and hence a cross comparison of proton heating in different codes. We now describe the measures for intermittency and wave physics.

- Omnidirectional spectra of magnetic field in the plane perpendicular to the mean field, i.e. $E_b(k_{\perp})$ where E_b is total magnetic energy in shells around k_{\perp} , should also be compared from all the models.

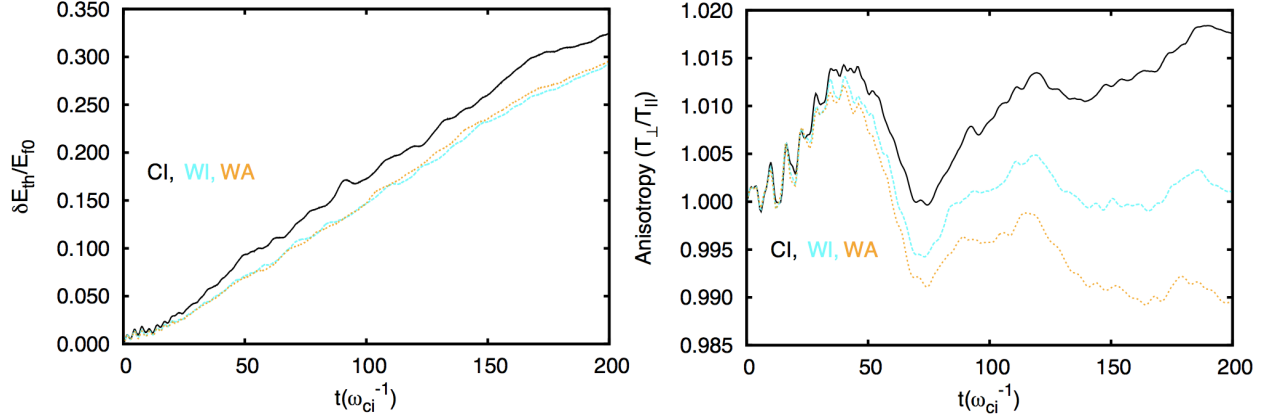


Figure 2: Change in thermal energy as fraction of initially available free energy as well as the anisotropy of proton heating for three hybrid simulations of OTV with: cold isothermal (CI), warm isothermal (WI) and warm adiabatic (WA) electrons. The system is turbulent after $t \sim 70$. In the turbulent regime, $\delta E_{th}/E_{f0}$ is almost the same for all three runs but the anisotropy is significantly different. From Parashar et al. (2014), Copyright American Institute of Physics.

4.1 Intermittent Structures

There are multiple different measures used to quantify intermittency of turbulence e.g. kurtosis of derivatives, scale dependent kurtosis, filtered kurtosis, probability distribution functions (PDFs) of increments, local intermittency measure (LIM), phase coherence index and partial variance of increments (PVI). Out of these, we will use scale dependent kurtosis and PDFs of increments. We describe these in a little more detail.

4.1.1 PDFs of Increments

The probability distribution functions (PDFs) of turbulent quantity are gaussian (e.g. Frisch (1996)) but the PDFs of increments of a turbulent quantity are not gaussian. By taking the increments, say for magnetic field, $\mathbf{B}(s + \delta s) - \mathbf{B}(s)$ we highlight the gradients (and hence the intermittent structures) in the quantity of interest. The strength of the gradients highlighted depends on the lag δs . Hence the increment for a smaller lag δs represents stronger gradients and hence most intermittent structures. When δs becomes comparable to the correlation length of the system, the PDFs revert back to gaussianity.

It has been shown that the non-gaussian tails on the PDFs of increments correspond to the number of intermittent structures (e.g. Greco et al. (2008); Salem et al. (2009); Greco et al. (2009); Wan et al. (2010)). Hence by comparing PDFs of a fixed increment ($\delta s \sim 1d_i$), from multiple models, we can compare the number of intermittent structures resolved in each model. This way, we can have a quantitative measure of intermittency as captured by different computational models.

4.1.2 Scale Dependent Kurtosis

The n^{th} order moment of the PDFs of a variable ϕ , also called Structure Functions, are defined as:

$$S_{\phi}^n(\ell) = \langle |\phi(x + \ell) - \phi(x)|^n \rangle = \langle \delta\phi_{\ell}^n \rangle. \quad (4)$$

The Kurtosis, the 4th order moment or 4th structure function, measures the Flatness of the PDFs of this given function ϕ . It is defined as:

$$\chi_{\phi} = \langle \delta\phi_{\ell}^4 \rangle / \langle \delta\phi_{\ell}^2 \rangle^2. \quad (5)$$

where ϕ is the quantity of interest, usually the current $\mathbf{j} = \nabla \times \mathbf{B}$ or the vorticity $\omega = \nabla \times \mathbf{v}$. It measures departures from Gaussianity. For a gaussian function its values is equal to 3 and is more for non-gaussian functions. Greater non-gaussianity is expected with smaller ℓ . A higher value of kurtosis reveals the presence of sharper concentrations of coherent structures. This is a straightforward diagnostic to implement on the simulation data and being a dimensionless ratio, should be independent of the units/normalizations used in the simulation codes.

4.1.3 Structure Functions and their scaling exponents

Within the inertial range, the structure functions defined in Eq.4 scale as power laws,

$$S_{\phi}^n(\ell) = \langle \delta\phi_{\ell}^n \rangle \propto \ell^{\zeta_n} \quad (6)$$

The scaling exponents ζ_n are classic measures of intermittency in hydrodynamic and MHD turbulence. Estimating the kurtosis (defined above) requires calculating structure functions up to the fourth order. When it is numerically feasible, it would be worthwhile to go up to sixth order and measure the first six scaling exponents for \mathbf{v} , \mathbf{B} , and \mathbf{n} over the scale range $2d_i < \ell < 20d_i$ in order to provide a more complete description of the intermittent fluctuations. Measuring these scaling exponents will also make it possible to tie into a larger literature on intermittency (e.g. Bruno and Carbone (2005); Salem et al. (2009); Chandran et al. (2014)). Structure Functions are also widely used in the analysis of solar wind fluctuations from spacecraft data, for both inertial range (e.g. Salem et al. (2009)) and dissipation range fluctuations (e.g. Osman et al. (2014)).

It will be important recognize that comparisons between codes and different runs is expected to become increasingly difficult for higher orders n . This is due not only to intrinsic statistical requirements, but also because higher order statistics (including kurtosis) are expected to vary with system size (see e.g., Anselmet et al. (1984)).

4.2 Wave Physics

The diagnostic to be used for wave physics will compare various wave properties. A few suggestions are:

4.2.1 Dispersion Analysis

An obvious test for the presence of waves is to look for the appropriate dispersion in the energy spectrum. A $k - \omega$ dispersion analysis of the simulation data will show excess of undamped energy along the dispersion curves of the normal modes of system. As an example figure 3 shows the spectrum of magnetic field as a function of k_{\parallel}, ω and k_{\perp}, ω from a 2.5D hybrid simulation with $\beta = 0.04$, large system size, mean field in the plane of simulation and driven at $|k| = 2, 3$ (from Parashar (2011)). The two-fluid dispersion curves for parallel and perpendicular propagation have been over-plotted. Outside the driving wave-numbers, there is clearly excess energy along the dispersion curves.

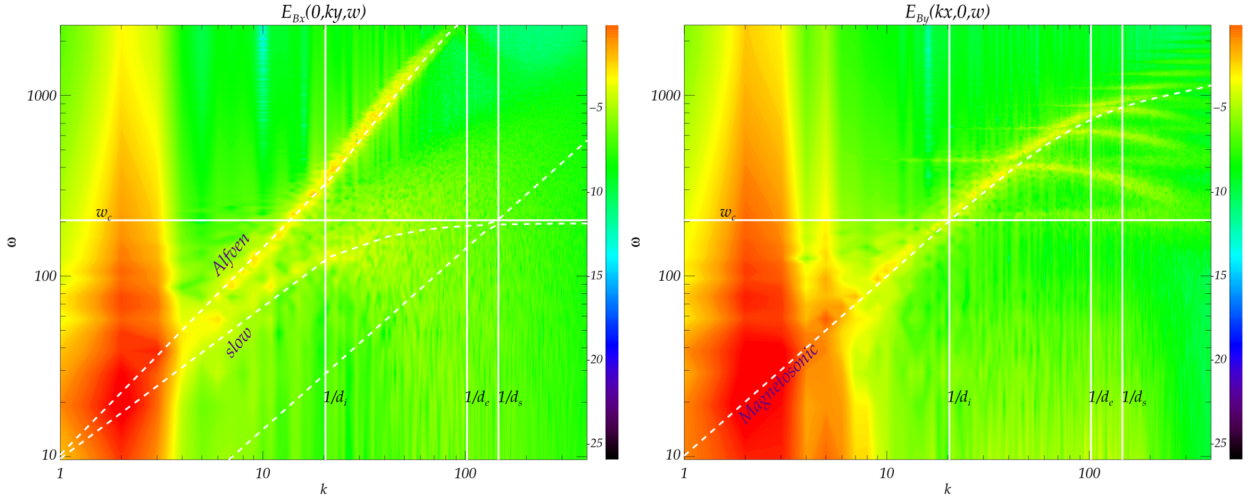


Figure 3: k, ω spectra of magnetic energy from a 2.5D hybrid PIC simulation, $\beta = 0.04$ driven at large scales of the system. The normal modes of the system are excited and we see excess energy along the dispersion curves of Alfvén, slow and magnetosonic modes. From Parashar (2011)

Hence k, ω diagrams are an important diagnostic to study the normal modes that survive in a simulation's evolution.

4.2.2 Damping Rate

One of the most important features to cross check is if the damping rate of the waves is appropriately captured by the simulation codes. The spectrum of waves has been chosen such that the damping rate is approximately the same for all the normal modes included in the initial condition. A comparison of numerically calculated damping rates to the average damping rate calculated from linear Vlasov theory is an important consistency check.

4.2.3 Compressibility

Two distinct compressibilities can be defined for a plasma (e.g. Gary and Smith (2009)). Compressibility of j th plasma species defined by:

$$C_j(\mathbf{k}) \equiv \frac{|\delta n(k)|^2}{n_0^2} \frac{B_0^2}{|\delta \mathbf{B}(k)|^2}$$

For a quasi-neutral plasma consisting of only electrons and protons, $C_e \sim C_p$, hence the compressibility of a only a single species can be considered. Along with plasma compressibility, the compressibility of magnetic field can also be computed:

$$C_{\parallel}(\mathbf{k}) \equiv \frac{|\delta B_{\parallel}(\mathbf{K})|^2}{|\delta \mathbf{B}(\mathbf{K})|^2}$$

The compressibility of the dominant modes (Alfvén-Kinetic Alfvén & Magnetosonic-Whistler) can be calculated from linear Vlasov theory and compared to simulations and observations (e.g. Gary and Smith (2009); Salem et al. (2012)). A direct comparison of the compressibility values expected from linear theory with the compressibilities captured by the simulations codes can serve as a test of code's capability of capturing the wave physics.

Indeed, the compressibility is a great test parameter to use for the identification of the dominant fluctuations or modes in the plasma. For instance, the compressibility of the Whistlers is constant in this range of scales/frequencies and depends on the angle of propagation of the mode (0 for parallel angles to 1 for quasi-perpendicular angles). As for the KAWs, the compressibility increases through the dissipation range, above the ion gyro-scale (eg. Salem et al. (2012)).

4.2.4 The Electric to Magnetic Field Ratio

The Electric to Magnetic Field ratio, $|\delta \mathbf{E}|/|\delta \mathbf{B}|$ (Salem et al. (2012)), provides a complementary test for wave-mode identification purposes. The $|\delta \mathbf{E}|/|\delta \mathbf{B}|$ ratio is constant in the inertial range as the electric and magnetic field fluctuations are well correlated (Bale et al. 2005). Indeed, the electric field \mathbf{E} in this range is essentially equivalent to $b f v \times \mathbf{B}$ (due to the incompressible nature of the Alfvénic fluctuations). Above the ion gyro-scale, $|\delta \mathbf{E}|/|\delta \mathbf{B}|$ increases as a function of k due to the dispersive nature of the modes. In linear theory, $|\delta \mathbf{E}|/|\delta \mathbf{B}|$ depends on the propagation angle of the mode, both in the inertial and dissipation range.

Like for the compressibility, a direct comparison of the $|\delta \mathbf{E}|/|\delta \mathbf{B}|$ expected from linear Vlasov-Maxwell theory with the $|\delta \mathbf{E}|/|\delta \mathbf{B}|$ captured by the simulations will be a useful tool to understand the nature of the fluctuations. Simulations show a very similar behavior of the $|\delta \mathbf{E}|/|\delta \mathbf{B}|$ obtained from observations or from linear theory. Quantifying those similarities and differences will be interesting.

4.3 Comparison to Observations

Although at this initial stage, we can not expect to see a direct comparison with realistic observations, it will still be instructive to take artificial cuts across simulations and compare the results to solar wind observations. These “artificial observations” can be provided to observers for comparisons with solar wind observations. Quantities like magnetic power spectra, compressibilities as well as correlations between different quantities such as reduced energy and cross helicity calculated from artificial observations can be compared to real observations.

This will help set up the communication between simulation modelers and the observers for future “critical simulations”.

5 Conclusion

A quantitative improvement in our understanding of the dissipative processes active in the solar wind requires as a first step, an understanding of the best available simulation models. To do so, we propose as a first step, a comparison of the capability of these codes to capture the essential underlying physics of collisionless turbulent plasmas.

We propose to compare how well different simulation models capture intermittency and also wave damping (where applicable). A set of initial conditions and common diagnostics have been proposed that will enable a quantitative cross-model comparison.

Based on the outcome of these simulations, we can decide on doing some “critical simulations”. These simulations will be the largest possible simulations with initial conditions designed to mimic real solar wind conditions. The data obtained from these simulations will be made open to the public for doing a quantitative comparison between different dissipative processes.

A Wave vectors for the KAW runs

-- Dispersion

ka_i	kc/wpi	theta	om_r/0m_ci	g/0m_ci	zero	om/kvA	g/om_r
0.275	0.502	84.83	0.0462	-5.511E-04	4.40E-12	0.0919	-0.012
0.357	0.652	85.60	0.0519	-1.020E-03	1.68E-10	0.0796	-0.020
0.439	0.802	86.42	0.0531	-1.534E-03	1.19E-10	0.0663	-0.029
0.521	0.951	86.99	0.0546	-2.144E-03	6.29E-11	0.0574	-0.039
0.603	1.101	87.40	0.0563	-2.844E-03	2.44E-11	0.0512	-0.050
0.685	1.251	87.71	0.0583	-3.626E-03	6.85E-12	0.0466	-0.062
0.767	1.401	87.95	0.0606	-4.481E-03	1.31E-12	0.0432	-0.074
0.849	1.551	88.15	0.0631	-5.402E-03	2.12E-09	0.0407	-0.086

-- Electric Field

kc/wpi	theta	(E_x/Etot)^2	(E_y/Etot)^2	(E_z/Etot)^2	(E_l/Etot)^2	(Etot/Btot)^2
0.5025	84.83	2.527E-04	9.997E-01	1.791E-05	9.910E-01	4.162E-03

0.6519	85.60	3.231E-04	9.996E-01	3.656E-05	9.930E-01	4.028E-03
0.8016	86.42	3.411E-04	9.996E-01	5.481E-05	9.950E-01	3.876E-03
0.9513	86.99	3.609E-04	9.996E-01	7.627E-05	9.961E-01	3.713E-03
1.1011	87.40	3.819E-04	9.995E-01	1.003E-04	9.967E-01	3.549E-03
1.2510	87.71	4.030E-04	9.995E-01	1.258E-04	9.971E-01	3.394E-03
1.4009	87.95	4.225E-04	9.994E-01	1.514E-04	9.974E-01	3.258E-03
1.5508	88.15	4.382E-04	9.994E-01	1.754E-04	9.977E-01	3.151E-03

-- E/B

kc/wpi	theta	(E_x/Btot)^2	(E_y/Btot)^2	(E_z/Btot)^2	(E_k/Btot)^2	(E_kB/Btot)^2
0.5025	84.83	1.052E-06	4.161E-03	7.455E-08	4.124E-03	3.647E-05
0.6519	85.60	1.302E-06	4.027E-03	1.473E-07	4.000E-03	2.690E-05
0.8016	86.42	1.322E-06	3.875E-03	2.125E-07	3.857E-03	1.822E-05
0.9513	86.99	1.340E-06	3.712E-03	2.832E-07	3.698E-03	1.332E-05
1.1011	87.40	1.355E-06	3.547E-03	3.559E-07	3.537E-03	1.031E-05
1.2510	87.71	1.368E-06	3.392E-03	4.270E-07	3.384E-03	8.329E-06
1.4009	87.95	1.377E-06	3.256E-03	4.933E-07	3.250E-03	6.977E-06
1.5508	88.15	1.381E-06	3.149E-03	5.527E-07	3.144E-03	6.025E-06

-- B

kc/wpi	theta	(B_x/Btot)^2	(B_y/Btot)^2	(B_z/Btot)^2	(B_z/E_z)^2
0.5025	84.83	9.720E-01	2.276E-04	2.780E-02	3.729E+05
0.6519	85.60	9.538E-01	2.715E-04	4.589E-02	3.116E+05
0.8016	86.42	9.323E-01	2.633E-04	6.740E-02	3.172E+05
0.9513	86.99	9.086E-01	2.525E-04	9.114E-02	3.218E+05
1.1011	87.40	8.838E-01	2.397E-04	1.160E-01	3.259E+05
1.2510	87.71	8.589E-01	2.253E-04	1.408E-01	3.299E+05
1.4009	87.95	8.352E-01	2.099E-04	1.646E-01	3.336E+05
1.5508	88.15	8.135E-01	1.938E-04	1.863E-01	3.370E+05

-- V (V_i - first line, V_e - second line)

kc/wpi	(dvx/dBtot)^2	(dvy/dBtot)^2	(dvz/dBtot)^2	(dv_k/dBtot)^2	(dv_kB/dBtot)^2
0.5025	0.85	8.212E-04	7.745E-03	6.524E-04	7.914E-03
0.5025	1.01	2.500E-04	2.097E-01	6.623E-04	2.093E-01
0.6519	0.77	9.647E-04	1.178E-02	7.953E-04	1.195E-02
0.6519	1.04	3.089E-04	3.553E-01	8.074E-04	3.548E-01
0.8016	0.68	9.231E-04	1.569E-02	7.964E-04	1.582E-02
0.8016	1.06	3.131E-04	5.411E-01	8.085E-04	5.406E-01
0.9513	0.58	8.800E-04	1.905E-02	7.982E-04	1.913E-02
0.9513	1.10	3.165E-04	7.673E-01	8.104E-04	7.668E-01
1.1011	0.48	8.366E-04	2.149E-02	7.996E-04	2.152E-02

1.1011	1.14	3.194E-04	1.034E+00	8.120E-04	1.033E+00
1.2510	0.39	7.949E-04	2.280E-02	7.994E-04	2.279E-02
1.2510	1.19	3.214E-04	1.339E+00	8.120E-04	1.339E+00
1.4009	0.30	7.566E-04	2.293E-02	7.970E-04	2.289E-02
1.4009	1.25	3.227E-04	1.681E+00	8.098E-04	1.680E+00
1.5508	0.23	7.234E-04	2.199E-02	7.919E-04	2.192E-02
1.5508	1.33	3.228E-04	2.054E+00	8.051E-04	2.054E+00

References

- Alexandrova, O., C. Lacombe, A. Mangeney, R. Grappin, and M. Maksimovic, 2012: Solar wind turbulent spectrum at plasma kinetic scales. *The Astrophysical Journal*, **760(2)**, 121.
- Anselmet, F., Y. Gagne, E. J. Hopfinger, and R. A. Antonia, 1984: High-order velocity structure functions in turbulent shear flows. *Journal of Fluid Mechanics*, **140**, 63–89.
- Bale, S. D., P. J. Kellogg, F. S. Mozer, T. S. Horbury, and H. Reme, 2005: Measurement of the electric fluctuation spectrum of magnetohydrodynamic turbulence. *Phys. Rev. Lett.*, **94(21)**, 215002.
- Bourouaine, S. and B. D. Chandran, 2013: Observational test of stochastic heating in low- β fast-solar-wind streams. *The Astrophysical Journal*, **774(2)**, 96.
- Bruno, R. and V. Carbone, 2005: The solar wind as a turbulence laboratory. *Living Reviews in Solar Physics*, **2(4)**.
- Chandran, B. D., A. A. Schekochihin, and A. Mallet, 2014: Intermittency and alignment in strong rmhd turbulence. *arXiv preprint arXiv:1403.6354*.
- Chandran, B. D. G., B. Li, B. N. Rogers, E. Quataert, and K. Germaschewski, 2010: Perpendicular ion heating by low-frequency alfvén-wave turbulence in the solar wind. *The Astrophysical Journal*, **720(1)**, 503.
- Chandrasekhar, S., 1961: Hydrodynamic and hydromagnetic stability. *International Series of Monographs on Physics, Oxford: Clarendon, 1961, 1*.
- Coleman, P. J., Jr., 1968: Turbulence, Viscosity, and Dissipation in the Solar-Wind Plasma. *The Astrophysical Journal*, **153**, 371–+.
- Frisch, U., 1996: *Turbulence*. Cambridge University Press.
- Gary, S., 2005: *Theory of space plasma microinstabilities*. Cambridge University Press, ISBN 0521437482.

- Gary, S. and C. Smith, 2009: Short-wavelength turbulence in the solar wind: Linear theory of whistler and kinetic Alfvén fluctuations. *Journal of Geophysical Research*, **114(A12)**, A12105.
- Gary, S. P., 1986: Low-frequency waves in a high-beta collisionless plasma polarization, compressibility and helicity. *Journal of plasma physics*, **35**, 431–447.
- Gary, S. P. and K. Nishimura, 2004: Kinetic alfvén waves: Linear theory and a particle-in-cell simulation. *Journal of Geophysical Research: Space Physics (1978–2012)*, **109(A2)**.
- Gary, S. P., S. Saito, and H. Li, 2008: Cascade of whistler turbulence: Particle-in-cell simulations. *Geophysical Research Letters*, **35(2)**, L02104+.
- Goldstein, M. L., D. A. Roberts, and W. H. Matthaeus, 1995: Magnetohydrodynamic Turbulence In The Solar Wind. *Annual Reviews of Astronomy & Astrophysics*, **33**, 283–326.
- Greco, A., P. Chuychai, W. H. Matthaeus, S. Servidio, and P. Dmitruk, 2008: Intermittent MHD structures and classical discontinuities. *Geophysical Research Letters*, **35**, 19111–+.
- Greco, A., W. H. Matthaeus, S. Servidio, P. Chuychai, and P. Dmitruk, 2009: Statistical analysis of discontinuities in solar wind ace data and comparison with intermittent mhd turbulence. *The Astrophysical Journal Letters*, **691(2)**, L111.
- He, J., C. Tu, E. Marsch, and S. Yao, 2012: Do oblique alfvén/ion-cyclotron or fast-mode/whistler waves dominate the dissipation of solar wind turbulence near the proton inertial length? *The Astrophysical Journal Letters*, **745(1)**, L8.
- Hollweg, J. and P. Isenberg, 2002: Generation of the fast solar wind: A review with emphasis on the resonant cyclotron interaction. *Journal of Geophysical Research*, **107(A7)**, 1147.
- Howes, G., W. Dorland, S. Cowley, G. Hammett, E. Quataert, A. Schekochihin, and T. Tatsuno, 2008: Kinetic Simulations of Magnetized Turbulence in Astrophysical Plasmas. *Physical Review Letters*, **100(6)**, 065004.
- Karimabadi, H., V. Roytershteyn, M. Wan, W. Matthaeus, W. Daughton, P. Wu, M. Shay, B. Loring, J. Borovsky, E. Leonardis, et al., 2013: Coherent structures, intermittent turbulence, and dissipation in high-temperature plasmas. *Physics of Plasmas*, **20**, 012303.
- Kolmogorov, A., 1941: The Local Structure of Turbulence in Incompressible Viscous Fluid for Very Large Reynolds' Numbers. *Akademiia Nauk SSSR Doklady*, **30**, 301–305.
- Leamon, R., C. Smith, N. Ness, and H. Wong, 1999: Dissipation range dynamics: Kinetic Alfvén waves and the importance of β e. *Journal of Geophysical Research*, **104(A10)**, 22331.
- Marsch, E., 2006: Kinetic physics of the solar corona and solar wind. *Living Reviews in Solar Physics*, **3(1)**.

- Matthaeus, W. and M. Goldstein, 1982: Measurement of the rugged invariants of magnetohydrodynamic turbulence in the solar wind. *Journal of Geophysical Research*, **87(A8)**, 6011–6028.
- Miura, A. and P. Pritchett, 1982: Nonlocal stability analysis of the mhd kelvin-helmholtz instability in a compressible plasma. *Journal of Geophysical Research*, **87(A9)**, 7431–7444.
- Osman, K. T., K. H. Kiyani, S. C. Chapman, and B. Hnat, 2014: Anisotropic Intermittency of Magnetohydrodynamic Turbulence. *The Astrophysical Journal Letters*, **783**, L27.
- Osman, K. T., W. H. Matthaeus, A. Greco, and S. Servidio, 2011: Evidence for inhomogeneous heating in the solar wind. *The Astrophysical Journal Letters*, **727(1)**, L11.
- Parashar, T., S. Servidio, M. Shay, B. Breech, and W. Matthaeus, 2011: Effect of driving frequency on excitation of turbulence in a kinetic plasma. *Physics of Plasmas*, **18**, 092302.
- Parashar, T. N., 2011: *On kinetic dissipation in collisionless turbulent plasmas*. Ph.D. thesis, University of Delaware.
- Parashar, T. N. and C. Salem, 2013: Turbulent dissipation challenge: A community driven effort. *arXiv preprint arXiv:1303.0204*.
- Parashar, T. N., M. A. Shay, P. A. Cassak, and W. H. Matthaeus, 2009: Kinetic dissipation and anisotropic heating in a turbulent collisionless plasma. *Physics of Plasmas*, **16(3)**, 032310.
- Parashar, T. N., B. J. Vasquez, and S. A. Markovskii, 2014: The role of electron equation of state in heating partition of protons in a collisionless plasma. *Physics of Plasmas (1994-present)*, **21(2)**, –.
- Podesta, J., J. Borovsky, and S. Gary, 2010: A kinetic alfvén wave cascade subject to collisionless damping cannot reach electron scales in the solar wind at 1 au. *The Astrophysical Journal*, **712(1)**, 685.
- Sahraoui, F., M. Goldstein, G. Belmont, P. Canu, and L. Rezeau, 2010: Three dimensional anisotropic k spectra of turbulence at subproton scales in the solar wind. *Physical Review Letters*, **105(13)**, 131101.
- Sahraoui, F., M. Goldstein, P. Robert, and Y. Khotyaintsev, 2009: Evidence of a cascade and dissipation of solar-wind turbulence at the electron gyroscale. *Physical review letters*, **102(23)**, 231102.
- Salem, C., G. Howes, D. Sundkvist, S. Bale, C. Chaston, C. Chen, and F. Mozer, 2012: Identification of kinetic alfvén wave turbulence in the solar wind. *The Astrophysical Journal Letters*, **745(1)**, L9.
- Salem, C., A. Mangeney, S. Bale, and P. Veltri, 2009: Solar wind magnetohydrodynamics turbulence: anomalous scaling and role of intermittency. *The Astrophysical Journal*, **702(1)**, 537.

- Schekochihin, A., S. Cowley, W. Dorland, G. Hammett, G. Howes, E. Quataert, and T. Tatsuno, 2009: Astrophysical gyrokinetics: kinetic and fluid turbulent cascades in magnetized weakly collisional plasmas. *The Astrophysical Journal Supplement Series*, **182**, 310.
- Shaikh, D. and G. Zank, 2009: Spectral features of solar wind turbulent plasma. *Monthly Notices of the Royal Astronomical Society*, **400(4)**, 1881–1891.
- Sundkvist, D., A. Retinò, A. Vaivads, and S. D. Bale, 2007: Dissipation in Turbulent Plasma due to Reconnection in Thin Current Sheets. *Physical Review Letters*, **99(2)**, 025004–+.
- TenBarge, J., J. Podesta, K. Klein, and G. Howes, 2012: Interpreting magnetic variance anisotropy measurements in the solar wind. *The Astrophysical Journal*, **753(2)**, 107.
- Wan, M., W. Matthaeus, H. Karimabadi, V. Roytershteyn, M. Shay, P. Wu, W. Daughton, B. Loring, and S. Chapman, 2012: Intermittent dissipation at kinetic scales in collisionless plasma turbulence. *Physical Review Letters*, **109(19)**, 195001.
- Wan, M., S. Oughton, S. Servidio, and W. Matthaeus, 2010: On the accuracy of simulations of turbulence. *Physics of Plasmas*, **17**, 082308.
- Wang, C. and J. Richardson, 2001: Energy partition between solar wind protons and pickup ions in the distant heliosphere: A three-fluid approach. *Journal of Geophysical Research*, **106**, 29401–29408.
- Wicks, R. T., M. A. Forman, T. S. Horbury, and S. Oughton, 2012: Power anisotropy in the magnetic field power spectral tensor of solar wind turbulence. *The Astrophysical Journal*, **746(1)**, 103.
- Wicks, R. T., T. S. Horbury, C. H. K. Chen, and A. A. Schekochihin, 2010: Power and spectral index anisotropy of the entire inertial range of turbulence in the fast solar wind. *Monthly Notices of the Royal Astronomical Society: Letters*, **407(1)**, L31–L35.
- Wu, P., S. Perri, K. Osman, M. Wan, W. Matthaeus, M. Shay, M. Goldstein, H. Karimabadi, and S. Chapman, 2013: Intermittent heating in solar wind and kinetic simulations. *The Astrophysical Journal Letters*, **763(2)**, L30.
- Xia, Q., J. C. Perez, B. D. Chandran, and E. Quataert, 2013: Perpendicular ion heating by reduced magnetohydrodynamic turbulence. *The Astrophysical Journal*, **776(2)**, 90.